Wall-Resolved LES Study of Shaped-Hole Film Cooling Flow for Varying Hole Orientation

A. Cody Nunno*, Sicong Wu†, Mushin M. Ameen‡, Pinaki Pal§, and Prithwish Kundu¶
Energy Systems Division, Argonne National Laboratory, Lemont, IL 60439, USA

Ahmed Abouhussein‖ and Yulia T. Peet **
Arizona State University, Tempe, AZ 85287, USA

Michael M. Joly††
Raytheon Technologies Research Center, East Hartford, CT 06108, USA

Peter A. Cocks ‡‡
Pratt and Whitney, East Hartford, CT 06118, USA

This work presents the findings from a wall-resolved large-eddy simulation (WRLES) study of a canonical gas turbine film cooling configuration performed using a high-order spectral element computational fluid dynamics (CFD) solver known as Nek5000. In particular, flow over a flat plate with a single row of 7-7-7 shaped cooling holes (represented by a single hole with periodic boundary conditions in the spanwise direction) was examined. Numerical results for the baseline case comprised of blowing ratio (BR) of 2, density ratio of 1.6, inlet freestream Reynolds number of 6000, and 30° cooling hole orientation relative to the mean flow were compared with available experimental data. Thereafter, simulations for hole angles of 25°, 35°, and 40° were performed (at BR = 2) to analyze the impact of hole orientation on the adiabatic cooling effectiveness profiles; blowing ratio was also varied (keeping the cooling hole angle fixed at 30°) to investigate its impact on adiabatic effectiveness. With respect to cooling hole angle, it was found that the 30° case had the best peak cooling effectiveness, whereas the 25° case exhibited a broader effectiveness profile with a lower peak due to the plenum flow being more aligned with the bulk flow. On the other hand, lower blowing ratio cases showed a wider film cooling effectiveness profile, but lower overall cooling effectiveness downstream of the cooling hole due to the specifics of the chosen configuration.

I. Nomenclature

BR	=	Blowing ratio
CFL	=	Courant–Friedrichs–Lewy number
D	=	Hole diameter
DNS	=	Direct numerical simulation
DR	=	Density ratio
FTT	=	Flow-through time
LES	=	Large-eddy simulation
T	=	Temperature
RANS	=	Reynolds-averaged Navier-Stokes

*Postdoctoral Appointee, 9700 South Cass Ave, Lemont, IL 60439.
†Postdoctoral Appointee, 9700 South Cass Ave, Lemont, IL 60439.
‡Research Scientist, 9700 South Cass Ave, Lemont, IL 60439.
§Research Scientist, 9700 South Cass Ave, Lemont, IL 60439, AIAA Member.
¶Research Scientist, 9700 South Cass Ave, Lemont, IL 60439.
‖Graduate Researcher, 501 E. Tyler Mall, Tempe, AZ 85287.
**Associate Professor, School for Engineering of Matter, Transport and Energy, 501 E. Tyler Mall, Tempe, AZ 85287, AIAA Member.
††Research Engineer, 411 Silver Lane, East Hartford, CT 06108.
‡‡Deputy Program Chief Engineer, 400 Main St, East Hartford, CT 06118, AIAA member.

Re_D = Reynolds number based on hole diameter
η = Film cooling effectiveness
θ = Normalized temperature

II. Introduction

Gas turbines require a high combustor exit temperature in order to be efficient. However, most gas turbine components past the combustor exit cannot withstand the necessary high temperatures for very long. Therefore, effective turbine cooling strategies are needed. Film cooling is a common approach, whereby air from the compressor stage is injected at the surface of the parts in question to create a barrier between the high temperature gases and the sensitive hardware. While film cooling has been a common practice for decades, understanding of the phenomenon is still imperfect, largely because of the challenges presented by experiments in such harsh conditions. By simulating such a flow, the authors seek to gain further insights into the film cooling phenomena.

Film cooling has been extensively studied via experiments in the past [1], but simulations have recently become a common means of examining these flows. Reynolds-Averaged Navier-Stokes (RANS) simulations have been commonly used for these studies [2, 3] due to low computational cost. However, due to the limits of the RANS turbulence modeling approach, it tends to be a poor predictor for parameters like adiabatic effectiveness [4–6]. Other methods have been used to improve upon these predictions. RANS hybridized with other models have become popular, using techniques like unsteady RANS or Detached Eddy Simulation [7, 8]. Large-eddy simulation (LES), though, has become the preferred simulation tool for studying film cooling effectiveness at lower cost than direct numerical simulation (DNS).

LES studies have been conducted for a variety of hole configurations. The simplest configuration that has been frequently studied is the cylindrical hole configuration [5, 9–11]. The main issue with cylindrical hole configurations is that they tend to inject the cooling fluid further into the boundary layer, thereby reducing the fluid's contact with the surface and thus cooling effectiveness. Shaped hole configurations, on the contrary, have been shown to generally have a better cooling effectiveness, as they diffuse the flow out of the hole better, and as a result are a significant geometry of study [12–18]. This work seeks to contribute to the existing body of literature on shaped hole film cooling by providing further high-fidelity simulation datasets.

Beyond hole shape, there are other features of the flow which can substantially affect the cooling effectiveness. Hole inclination angle has been occasionally studied [19–22], but investigations of its effects have been limited in scope and have rarely been simulated. Changes in blowing ratio also substantially alter cooling performance [23–25], with its results depending somewhat on the shape of the cooling hole configuration.

This manuscript summarizes a campaign of high-fidelity wall-resolved LES of shaped hole geometries at conditions relevant to film cooling, using implicit LES for a 7-7-7 shaped hole configuration previously considered by Oliver and coworkers [15]. Results of these simulations are compared to the previous experimental results for model verification and validation. Results for velocity and adiabatic film cooling effectiveness are compared qualitatively and quantitatively. Alterations to the configuration are then performed. Specifically, small adjustments are made to the angle of the cooling hole above and below the baseline configuration for comparison. Further configuration changes explored include altering the blowing ratio (BR) for the baseline 30° configuration.

III. Computational Configuration

First, the geometry used for the simulations is described. Then, the details of the simulation configuration are provided. Finally, adjustments made to the geometry and simulation configuration for the latter part of this work are outlined.

A. Simulation Geometry

The geometry simulated in this work is identical to the one considered in Oliver et al. [15]. It consists of three parts: a 7-7-7 shaped hole, a plenum feeding cooled air into the hole, and a flat plate acting as the surface to be cooled. The hole geometry details are described in Ref. [26]. The configuration initially examined has the hole entering the flat plate region at an angle of 30°. The original experiment's geometry was set up as a series of these cooling holes arranged in parallel, so as to mimic the cooling configurations typical of gas turbines.

The baseline flow configuration examined has a blowing ratio (BR) of 2.0, a density ratio (DR) of 1.6, a Reynolds number of 6000 based on the diameter of the hole (Re_D), and a freestream Mach number of approximately 0.15. The

plenum consists of a $16D \times 15D \times 6D$ box centered around the smaller end of the shaped hole. The flat plate region is described using a $25D \times 5D \times 6D$, where the hole enters the geometry approximately $5.2D$ downstream of the inlet, leaving a further $17.5D$ of the plate after the hole. An overview of this geometry can be seen in Fig. 1.

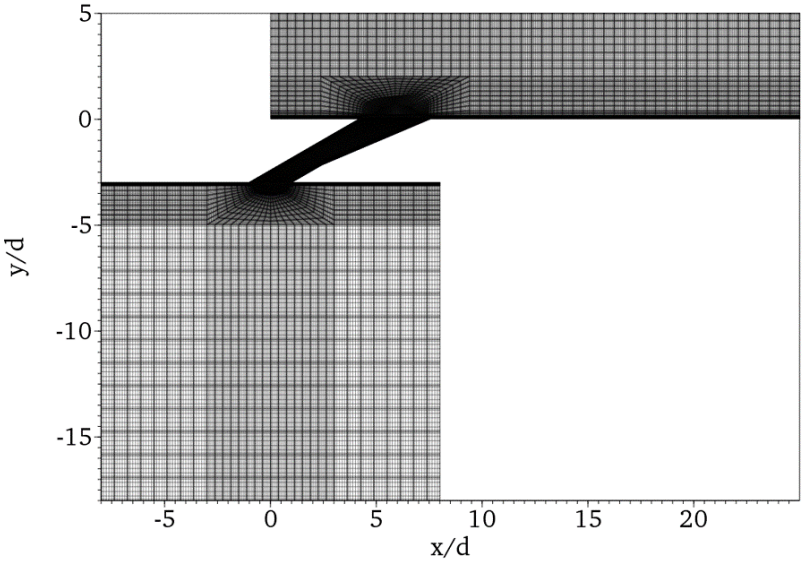

(a) Entire mesh

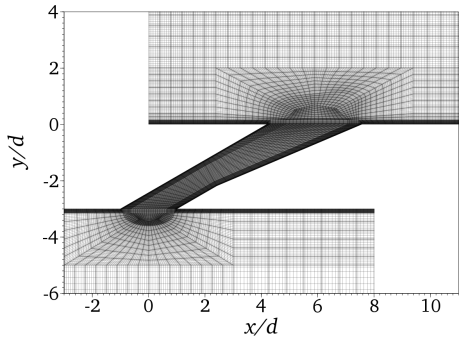

(b) Hole region mesh detail

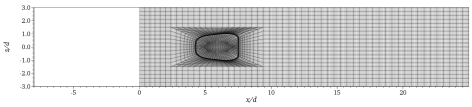

(c) Mesh detail of the flat plate region from above

Fig. 1 30° hole angle LES mesh with highlighted details.

B. Simulation Details

The flow was simulated using the Nek5000 [27] platform, a higher-order spectral element CFD code, using its low Mach flow solver. The simulation performed was an implicit, wall-resolved LES, using a high-pass filter with a relaxation term. The time scheme used was a semi-implicit second-order backward differentiation method with extrapolation using an operator-integrator factor scheme (OIFS). The grid was created to be fairly coarse for the 30° case, 105128 elements, with refinement coming from the eighth-order polynomials used over each element, creating an effective resolution of 53.8 million grid points. The grid is also more refined in locations of particular importance, such as inside the hole and near the wall in the flat plate region. An overview of the grid can be seen in Fig. 1.

A variable time-stepping scheme was used for these simulations, restricted such that $CFL \leq 1.5$, due to the use of OIFS. Time-averaged statistics for the flow were taken over 18.6 flow-through times after an initial phase of 1.4 flow-through times to establish an approximately steady flow. During this initial development phase, a more typical

time-stepping scheme is used, restricting the $CFL \leq 0.5$ for only the first 1.4 flow-through times. A flow-through time (FTT) in this work was based on the freestream velocity of the flat plate region, indicating the length of time for a theoretical fluid particle entering that region at the inflow boundary to travel to the outflow boundary.

C. Boundary Conditions

The incoming velocity profile over the flat plate was considered to be a Blasius boundary layer profile. Since Nek5000 uses a non-dimensional framework, velocity was used as the non-dimensionalizing parameter, such that the incoming freestream velocity over the flat plate region was equal to unity, given a Re_D of 6000. To match the BR in the plenum, a constant velocity inflow was applied at the bottom of the plenum, approximately 1.02% of the freestream velocity over the flat plate. The appropriate DR was achieved in the experiment using air at 295K in the boundary layer, and at 184K in the plenum region. Properties necessary to compute transport equations were taken from air at the appropriate temperature condition, then normalized.

The spanwise boundaries in Fig. 1a were periodic for this simulation, so as to model an infinite series of holes next to one another. The top boundary was open to allow flow to move freely out of the domain, as is the exit of the flat plate. The walls of the hole, plenum, and flat plate regions were all considered as adiabatic walls under the no-slip condition.

D. Geometry and Configuration Variations: Hole Angle and Blowing Ratio

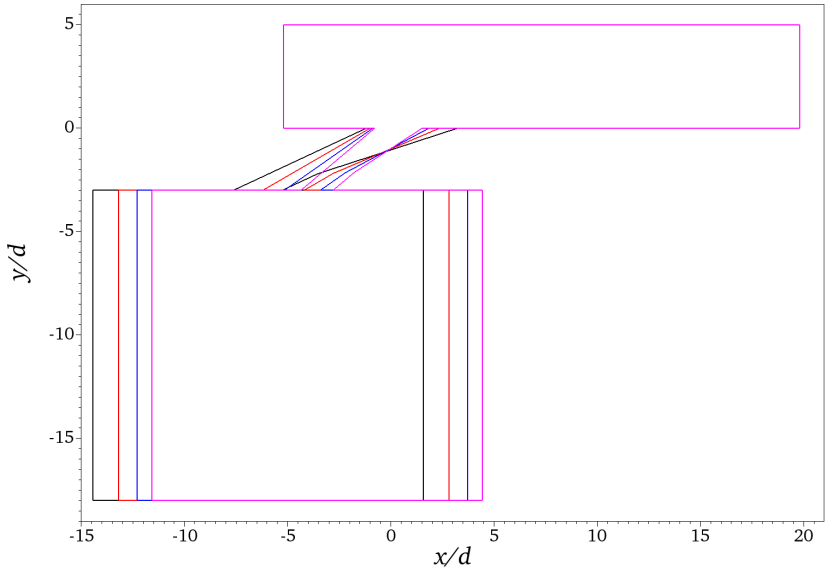

(a) Side view

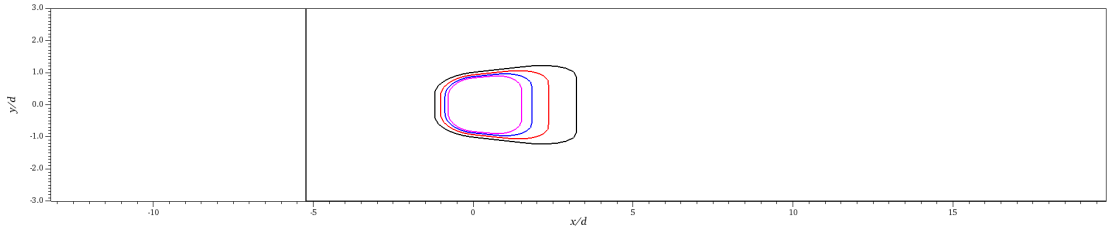

(b) Detail of the flat plate region from above

Fig. 2 Geometries with varying hole angles overlaid on one another for comparison. The 30° baseline geometry is outlined in red. 25°, 35°, and 40° geometries are outlined in black, blue, and magenta, respectively.

Two types of alterations were made to the Oliver et al. [15] flow configuration in the latter part of this work to examine their impact on cooling effectiveness. First, the angle of orientation of the hole relative to the flat plate region was adjusted through a series of angles surrounding the 30° baseline case. Then, the blowing ratio of the baseline case was decreased below $BR = 2.0$.

For the flow configurations in which the hole angle changes, most features of the geometry and flow (D, BR, DR, Re_D) remained consistent with the baseline case. The hole geometry angles examined in addition to the baseline 30° case were 25°, 35°, and 40°. These adjusted geometries can be seen in Fig. 2. The hole entry remains centered around the plenum, and the center of the hole exit is fixed to the same location in the flat plate region as it is for the 30° orientation; this can be seen in Fig. 2a. The adjusted exit profile of the hole results in changes to the length of the flat plate observable in the domain after the hole exit, as can be seen in Fig. 2b.

The last set of cases only adjusted the blowing ratio, down from 2.0 in a sweep of $BR = 0.5, 1.0, 1.5$. This was accomplished by adjusting the inflow velocity imposed at the bottom of the plenum to match the blowing ratio; thus, Re_D was kept the same as in the baseline case, as were density ratio and the hole configuration. The change in the blowing ratio relative to the freestream velocity allowed the maximum CFL considered to be increased to 2.0 for the $BR = 1.0$ and 1.5 cases, but the $BR = 0.5$ retained the same restrictions as the baseline case.

IV. Simulation Results

First, the 30° hole angle case was considered for simulation validation, comparing the current simulation results to the experimental data from Oliver et al. [15]. Then, the 25°, 30°, 35°, and 40° hole angle cases were compared, examining the change in film cooling effectiveness, η, due to the change in hole angle. Finally, the baseline case was compared to WRLES corresponding to decreasing blowing ratio to examine how film cooling effectiveness changes with this parameter.

A. Baseline Case: 30° Hole Angle

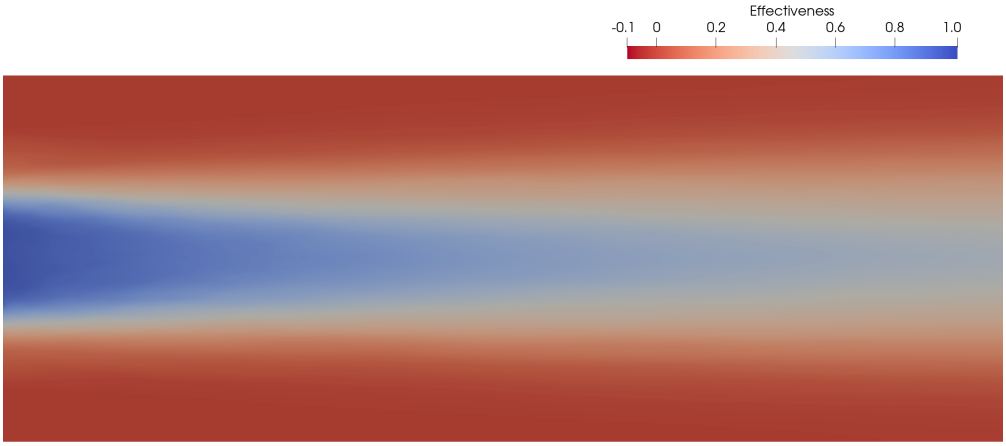

Fig. 3 Surface effectiveness η in the flat plate region for the baseline 30° WRLES.

Examining the cooling effectiveness on the surface of the flat plate region, the present simulation appears to match the experimental data quite well. The 2D plot of cooling effectiveness, shown in Fig. 3, visually matches the effectiveness data from Oliver and coworkers. This cooling effectiveness is defined as

$$\eta = \frac{T_\infty - T_w}{T_\infty - T_c}, \tag{1}$$

where T_∞ is the freestream temperature, T_c is the temperature of the coolant, and T_w is the local temperature at the wall. Generally, the contours of the surface effectiveness are approximately as broad as the previous experiment.

By examining 1D plots of surface effectiveness, a more quantitative comparison between the current simulation and experiments is possible. The centerline surface effectiveness can be seen in Fig. 4. Here, the present simulation matches the surface effectiveness of the experiments from the referenced work. Further evidence of the excellent match

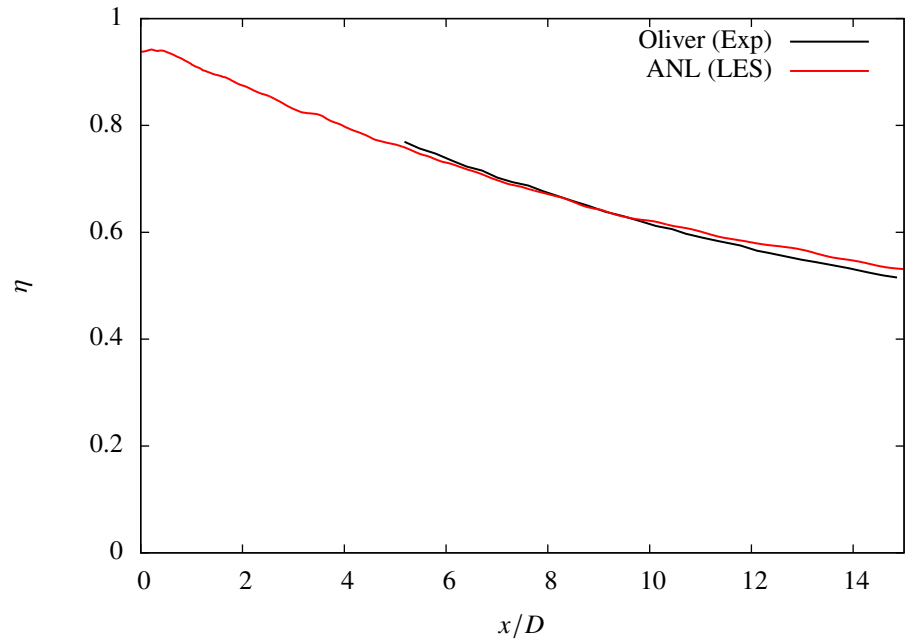

Fig. 4 Surface effectiveness η at the centerline in the flat plate region for the baseline 30° WRLES. The figure compares LES with experimental data from Oliver et al. [15]. x/D is measured from the downstream edge of the hole.

in cooling effectiveness can be seen in Fig. 5. Here, the "flattening" of the film cooling effectiveness profile can be more easily quantified than in Fig. 3; that is, peak cooling effectiveness is seen to decrease downstream in the simulation, but cooling effectiveness increases downstream at the edges of the wake region resulting from the cooling hole flow. The present LES shows approximately the same behavior as the experiment, matching closely at the various stations downstream of the hole. There is little discrepancy in the peak effectiveness near the center of the hole wake region. However, effectiveness is slightly higher than anticipated by the experiment at the distance furthest downstream.

Normalized temperature can also be compared to the previous work. Here, normalized temperature is defined as:

$$\theta = \frac{T_\infty - T}{T_\infty - T_c}\,, \tag{2}$$

where T is the local temperature, effectively the same non-dimensionalization as η. The heatmap for normalized temperature, shown in Fig. 6, indicates a strong similarity of the present simulation to the experiment [15]. Both the present simulation and the experiment exhibit a flat, ellipsoidal profile.

Normalized temperature can be measured more quantitatively using 1D data from the $x/d = 5$ plane. Here, θ profiles are shown at half diameter increments outward from the centerline along this plane. These comparisons are shown in Fig. 7. Nearer to the centerline, the comparisons are almost identical. In the more distant region, there is some small deviation from experiment, likely owing to the choice of subgrid model.

Fig. 8 shows the velocity profile both in the hole and over a small portion of the flat plate region. The velocity of the hole region matches the profile exhibited in Oliver and coworkers [15]: namely, a small recirculation region near the plenum entry, followed by an accelerated flow along the top of the hole. The velocity magnitudes in these two regions are approximately the same as the magnitudes shown in the previous work. The flat plate region also shows similar behavior to the previous work, in the form of a relatively swiftly developing boundary layer, propelled by the flow acceleration in the hole.

Root mean squared velocity is shown as a measurement of turbulence intensity in Fig. 9, and it provides a clearer picture of the mixing intensity in the hole region of the simulation. As can be seen from the three planes in the hole shown in the image, the turbulence intensity is highest at the sharp corner where the plenum meets the hole. This appears to create a band of high turbulence intensity that gets carried with the main flow through the hole, ascending from the bottom of the hole to the top as the flow in the hole mixes.

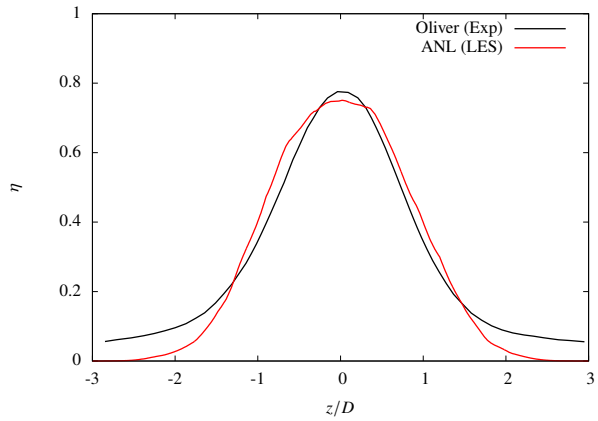

(a) $x/D = 5$

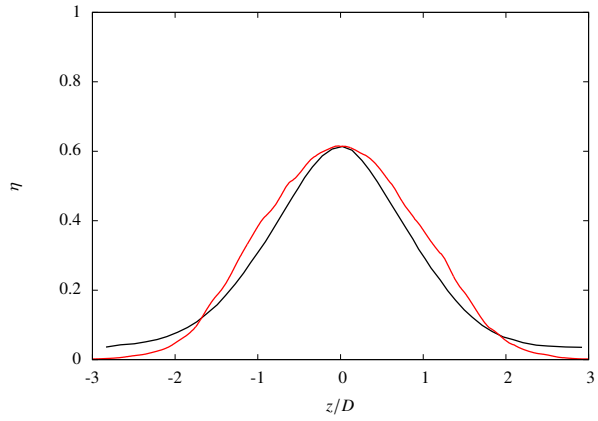

(b) $x/D = 10$

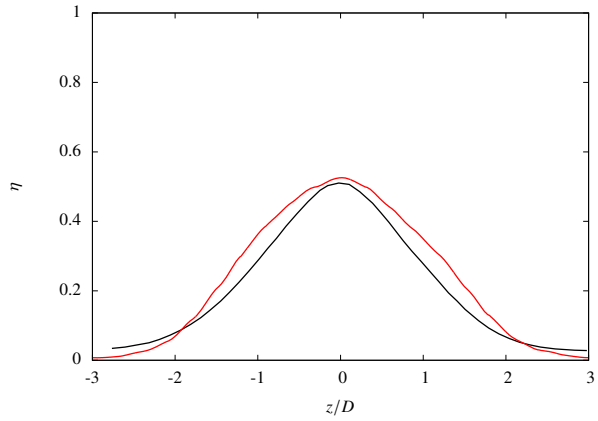

(c) $x/D = 15$

Fig. 5 Adiabatic effectiveness η over the span of the flat plate at various distances downstream of the hole for the baseline 30° WRLES. The figure compares LES with experimental data from Oliver et al. [15]. x/D is measured from the downstream edge of the hole.

B. Hole Angle Variation

In Fig. 10, the surface effectiveness contours for the 25°, 35°, and 40° LES cases (at BR = 2) are shown. Differences in both as compared to the 30° case are readily apparent. Fig. 10a (25°) has a slightly weaker effectiveness in the core of

Fig. 6 Normalized temperature θ in the flat plate region at $x/D = 5$ for the baseline 30° LES.

the hole's wake, but the effectiveness is much broader over the flat plate. Fig. 10b (35°) demonstrates the opposite trend: the effectiveness is fairly strong in the area immediately past the hole, but that effectiveness drops off fairly quickly, and cooling is not seen over a span of the flat plate nearly so broad as the 30° case. The same trend is visible and even more exaggerated in the 40°case (Fig. 10c), where the effectiveness drops off steeply.

These differences can be examined quantitatively by looking at cooling effectiveness plots similar to the ones in Figs. 11 and 5. Fig. 11 shows the centerline effectiveness for all four LES cases from the present study. The trends from the color plots are confirmed here: the peak effectiveness seen at the centerline wanes substantially in the 35° and 40° cases when compared with the 30° case, while the effectiveness is overall lower at the centerline for the 25° case. The trends are clearer in Fig. 12, which shows the effectiveness at various downstream locations. As compared to the 30° case, the 35° case exhibits inferior cooling effectiveness at the surface; across the entire flat plate region, the film cooling effectiveness for the 35° case is approximately 5% lower than the 30° case. The same trends are seen for the 40° case, only more so; the film cooling effectiveness for the 40° case is nearly 25% lower than the 30° case throughout the entire domain, except in the region directly downstream of the hole. The benefits of the more flow-aligned 25° hole angle case are evident; film cooling effectiveness is substantially greater than the 30° baseline across the flat plate region at the cost of some peak cooling effectiveness.

A visualization of the cooling capacity of each of these altered configurations is visible in Fig. 13. The 25° case (Fig.13a) is flatter against the surface of the wall than the 30° case due to the hole being more aligned with the flow, resulting in a higher overall cooling effectiveness; a more substantial portion of the flow is in contact with wall in the boundary layer. For the 35° (Fig.13b) and 40° (Fig.13c) cases, however, the fluid from the plenum injects substantially further into the boundary layer, causing the fluid to mix more with the bulk flow and resulting in less overall cooling of the surface of the wall.

C. Blowing Ratio Variation

Based on the surface plots of effectiveness in the 30° hole angle configuration for varying blowing ratio (Fig. 14), two trends are observed as the blowing ratio increases. First, the lower BR cases tend to have a wider film cooling profile as compared to the baseline case. This is also correlated to the cooling effectiveness immediately behind the hole, which is slightly higher in the $BR = 0.5$ case. Second, it's also notable how the cooling effectiveness significantly drops off as the flow moves downstream over the plate. This is presumably due to the decrease in the injected mass of the cold fluid as the blowing ratio decreases.

Figs. 15 and 16 show quantitative comparisons of the surface effectiveness with decreasing BR. The strong decrease in centerline cooling effectiveness can be seen in Fig. 15, where the lower BR cases begin at the same effectiveness as the baseline case (or slightly higher), but quickly become less effective. The increase in cooling profile width can be seen in Fig. 16. Here, it is evident that the cooling profile width is increased for lower BR cases as compared to the baseline, at least until the last downstream station is reached, where the width is approximately similar. Again, this is likely attributable to the decrease in cold fluid mass injected into the boundary layer in lower BR conditions.

The injected mass argument is even more compelling based on the normalized temperature data from Fig.17. Here, it is clear that much less cold fluid is making its way to the downstream stations along the plane, resulting in less fluid mass to cool the plate. The lower mass flow rate out of the hole relative to the bulk flow results in the cold fluid being more spread out along the cooled surface, but ultimately the flow has less total cooling power.

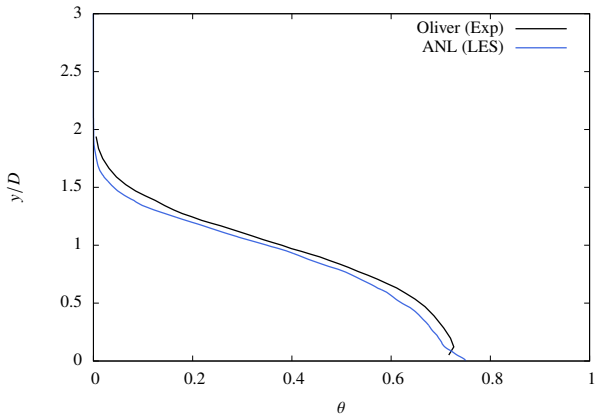

(a) $z/D = 0$

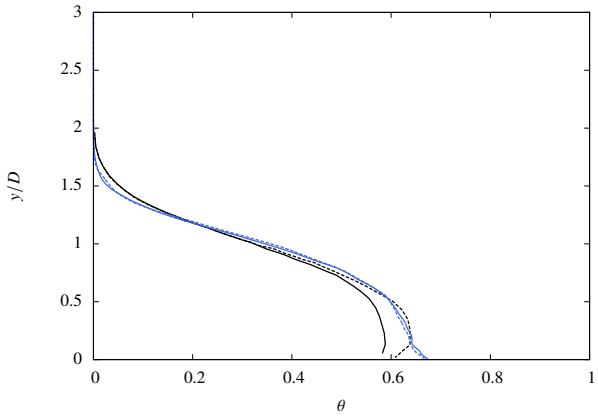

(b) $z/D = \pm 0.5$

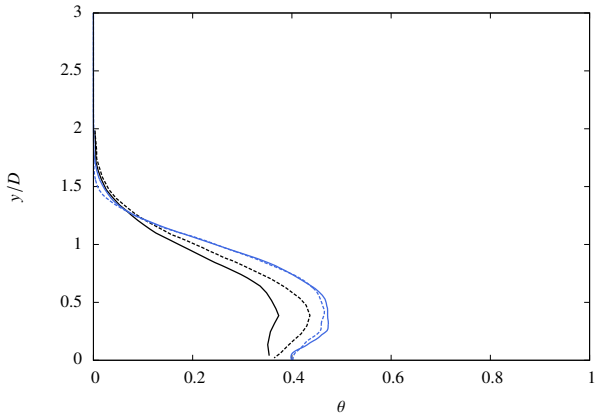

(c) $z/D = \pm 1$

Fig. 7 Normalized temperature θ over the span of the flat plate at a distance of $x/d = 5$ downstream from the hole for the baseline 30° LES. The figure compares LES with experimental data from Oliver et al. [15]. Solid lines in (b) and (c) refer to the right side of the symmetric domain ($z/D = +0.5$, $z/D = +1$), and dashed lines refer to the left side of the symmetric domain ($z/D = +0.5$, $z/D = -1$).

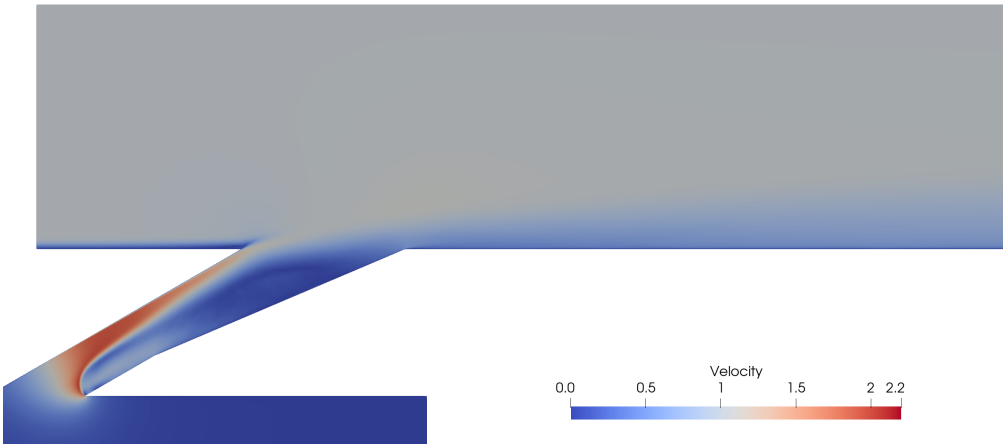

Fig. 8 Velocity profile in the hole and flat plate region for the baseline 30° LES.

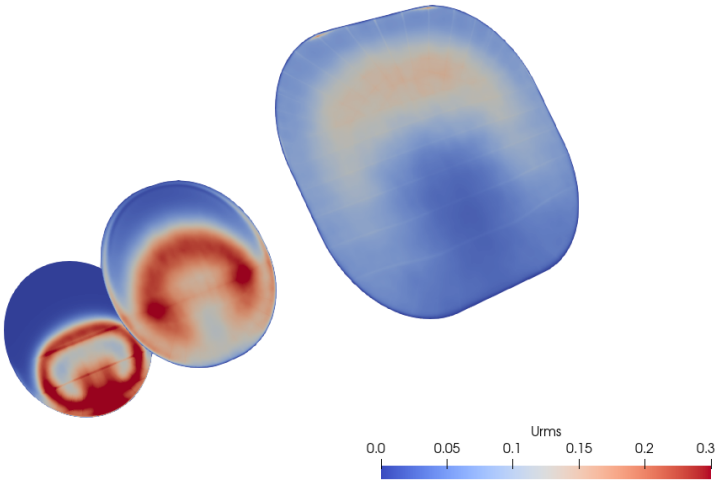

Fig. 9 Root mean squared velocity profile in the hole region for the baseline 30° LES.

V. Conclusions

In this work, an implicit WRLES exploration of the effects of cooling hole angle and blowing ratio on film cooling effectiveness has been performed on a 7-7-7 shaped hole configuration arranged to mimic an infinite series of cooling holes on a flat plate. The configuration was validated against previous experiments by Oliver et al. [15], showing performance comparable to both the experiment and previous simulations. By varying hole angle, cooling effectiveness was found to vary significantly; in general, flow from the holes which were more aligned with the bulk flow provided more cooling effectiveness along the plate surface. Hole angles which inject the flow up higher into the bulk flow were less effective at cooling the surface. Lower blowing ratios were less effective overall at cooling the boundary layer surface after the hole, but presented a wider overall cooling profile than the high blowing ratio.

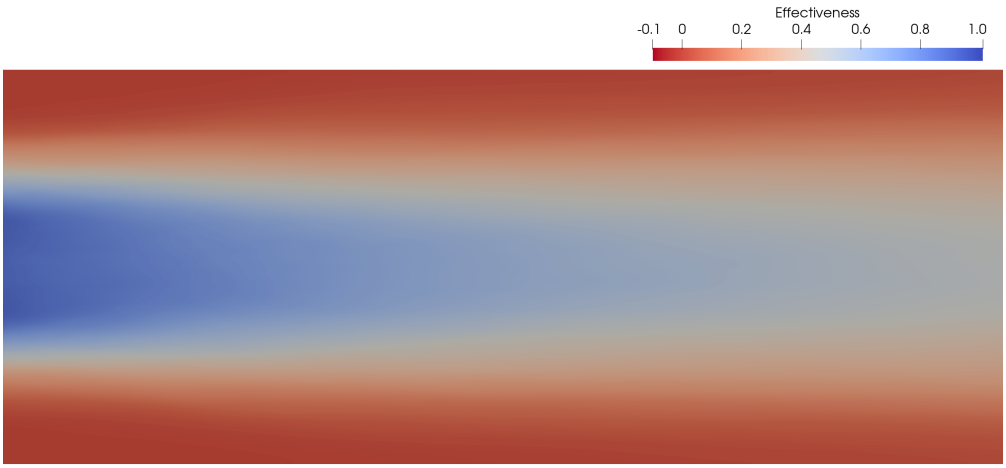

(a) 25°

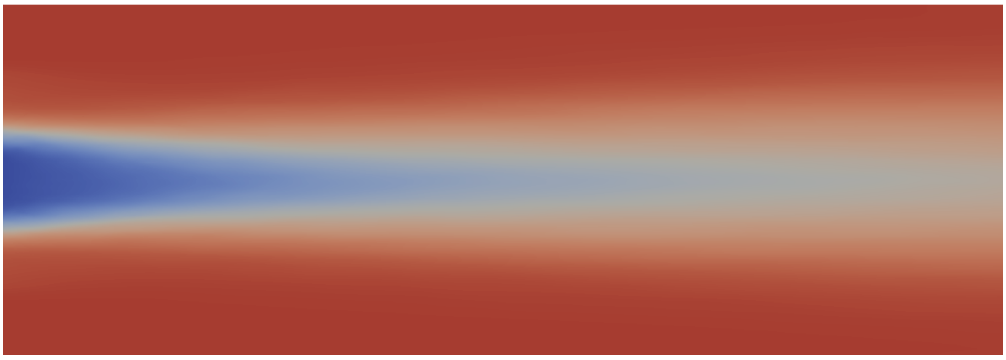

(b) 35°

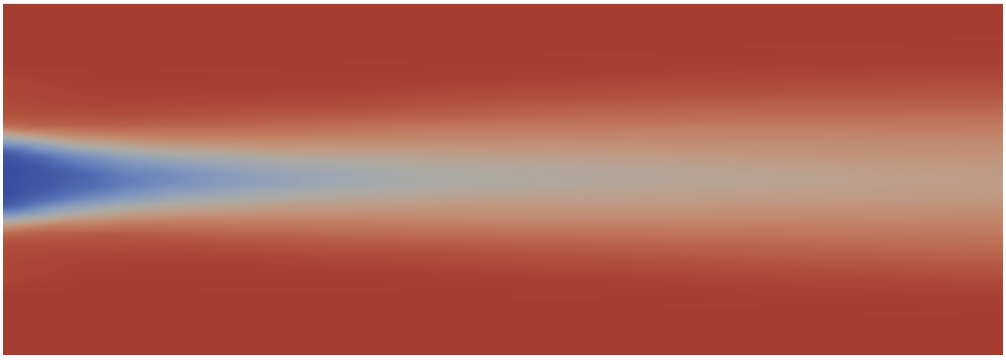

(c) 40°

Fig. 10 Surface effectiveness η in the flat plate region after the hole for LES cases at various hole angles.

VI. Future Work

A more complete sweep of the conditions surveyed will be completed to determine an optimal cooling hole orientation and blowing ratio combination. In addition, a machine-learned wall model is being developed from the high-fidelity WRLES data for this configuration to enable more cost-effective yet predictive wall-modeled LES (WMLES) of film cooling in the future.

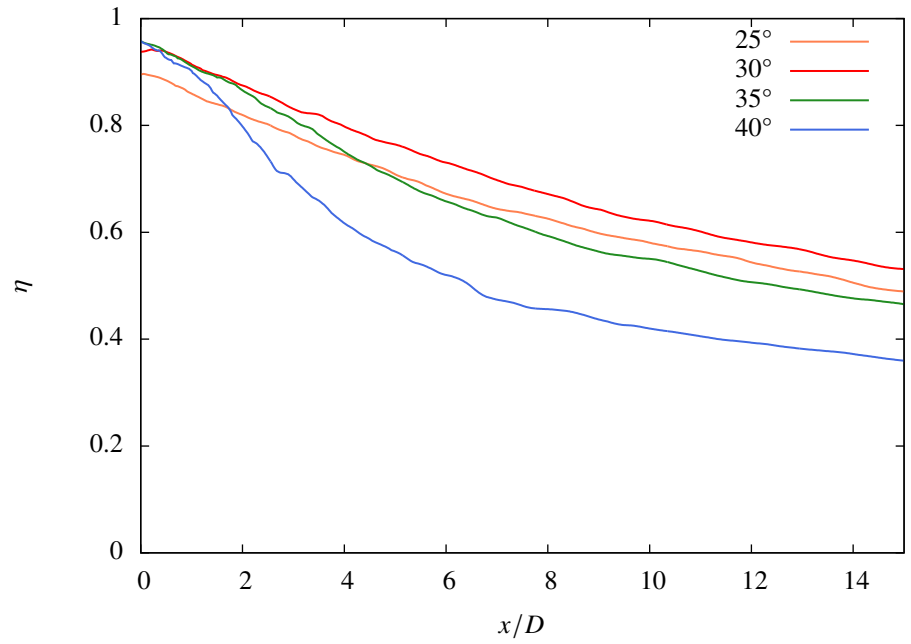

Fig. 11 Surface effectiveness η at the centerline in the flat plate region. The figure compares different hole angle configurations. x/D is measured from the downstream edge of the hole.

VII. Acknowledgements

The submitted manuscript has been created by UChicago Argonne, LLC, Operator of Argonne National Laboratory (Argonne). Argonne, a U.S. Department of Energy Office of Science laboratory, is operated under Contract No. DEAC02-06CH11357. The U.S. Government retains for itself, and others acting on its behalf, a paid-up nonexclusive, irrevocable worldwide license in said article to reproduce, prepare derivative works, distribute copies to the public, and perform publicly and display publicly, by or on behalf of the Government. The research work was funded by the DOE Advanced Manufacturing Office (AMO) through the High Performance Computing for Energy Innovation (HPC4EI) program. The authors thank Dr. Robert Shroeder from Sargent and Lundy and Prof. Karen Thole from Pennsylvania State University for sharing the CAD file of the 7-7-7 shaped hole configuration. Lastly, the authors would like to acknowledge the computing core hours available through the Bebop cluster provided by the Laboratory Computing Resource Center (LCRC) at Argonne National Laboratory and National Energy Research Scientific Computing Center (NERSC) Cori supercomputer for this research.

References

[1] Bogard, D. G., and Thole, K. A., "Gas turbine film cooling," *Journal of propulsion and power*, Vol. 22, No. 2, 2006, pp. 249–270.

[2] Ling, J., Elkins, C. J., and Eaton, J. K., "Optimal Turbulent Schmidt Number for RANS Modeling of Trailing Edge Slot Film Cooling," *Journal of Engineering for Gas Turbines and Power*, Vol. 137, No. 7, 2015, p. 072605.

[3] Jiang, Y., Murray, A., di Mare, L., and Ireland, P., "Mesh sensitivity of RANS simulations on film cooling flow," *International Journal of Heat and Mass Transfer*, Vol. 182, 2022, p. 121825.

[4] Acharya, S., Tyagi, M., Hoda, A., et al., "Flow and heat transfer predictions for film cooling," *Annals-New York Academy of Sciences*, Vol. 934, 2001, pp. 110–125.

[5] Peet, Y. V., and Lele, S. K., "Near field of film cooling jet issued into a flat plate boundary layer: LES study," *Turbo Expo: Power for Land, Sea, and Air*, Vol. 43147, 2008, pp. 409–418.

[6] Haydt, S., Lynch, S., and Lewis, S., "The effect of a meter-diffuser offset on shaped film cooling hole adiabatic effectiveness," *Journal of Turbomachinery*, Vol. 139, No. 9, 2017.

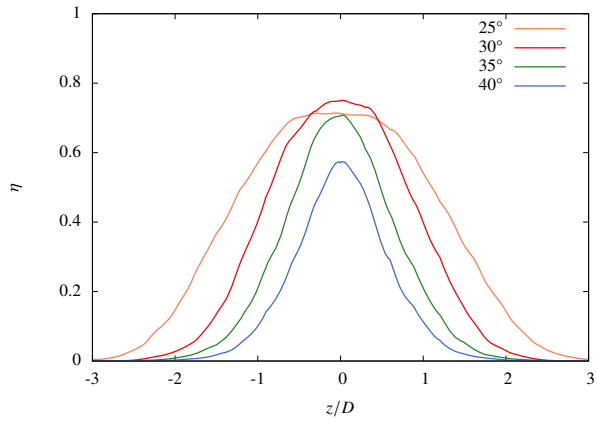

(a) $x/D = 5$

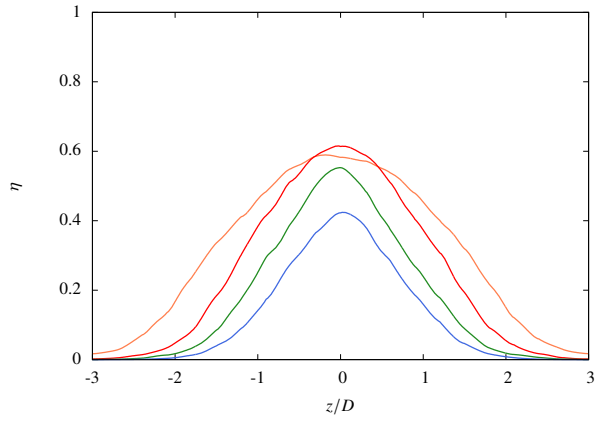

(b) $x/D = 10$

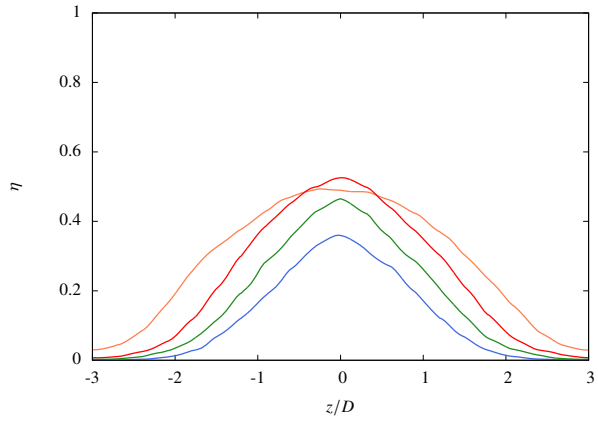

(c) $x/D = 15$

Fig. 12 Adiabatic effectiveness η over the span of the flat plate at various distances downstream of the hole. The figure compares different hole angle configurations. x/D is measured from the downstream edge of the hole.

[7] Takahashi, T., Funazaki, K.-i., Salleh, H. B., Sakai, E., and Watanabe, K., "Assessment of URANS and DES for prediction of leading edge film cooling," *Journal of Turbomachinery*, Vol. 134, 2012, pp. 031008–1.

[8] Foroutan, H., and Yavuzkurt, S., "Numerical simulations of the near-field region of film cooling jets under high free stream

(a) 25°

(b) 35°

(c) 40°

Fig. 13 Normalized temperature θ in the flat plate region at $x/D = 5$ for various hole angles.

turbulence: application of RANS and hybrid URANS/large eddy simulation models," *Journal of Heat Transfer*, Vol. 137, No. 1, 2015.

[9] Iourokina, I. V., and Lele, S. K., "Large eddy simulation of film cooling flow above a flat plate from inclined cylindrical holes," *Fluids Engineering Division Summer Meeting*, Vol. 47500, 2006, pp. 817–825.

[10] Johnson, P. L., and Shyam, V., *Large eddy simulation of a film cooling flow injected from an inclined discrete cylindrical hole into a crossflow with zero-pressure gradient turbulent boundary layer*, National Aeronautics and Space Administration, Glenn Research Center, 2012.

[11] Bodart, J., Coletti, F., Bermejo-Moreno, I., and Eaton, J., "High-fidelity simulation of a turbulent inclined jet in a crossflow," *Center for Turbulence Research Annual Research Briefs*, Vol. 19, 2013, pp. 263–275.

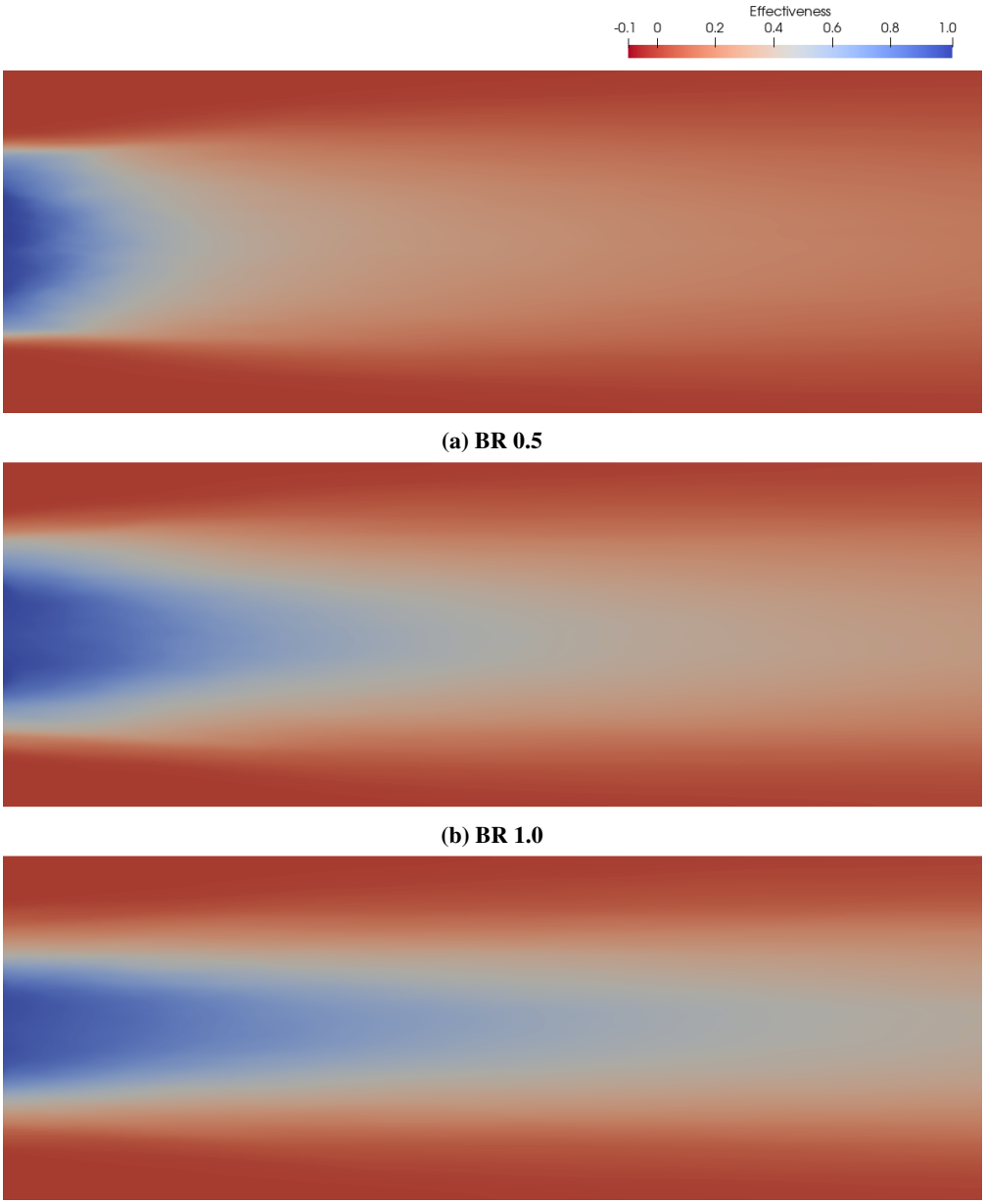

(a) BR 0.5

(b) BR 1.0

(c) BR 1.5

Fig. 14 Surface effectiveness η in the flat plate region for LES cases at various blowing ratios.

[12] Leedom, D., and Acharya, S., "Large eddy simulations of film cooling flow fields from cylindrical and shaped holes," *Turbo Expo: Power for Land, Sea, and Air*, Vol. 43147, 2008, pp. 865–877.

[13] Konopka, M., Jessen, W., Meinke, M., and Schröder, W., "Large-eddy simulation of film cooling in an adverse pressure gradient flow," *Journal of Turbomachinery*, Vol. 135, No. 3, 2013.

[14] Zhong, L., Zhou, C., and Chen, S., "Large eddy simulation of inclined jet in cross flow with cylindrical and fan-shaped holes," *ASME Turbo Expo 2016: Turbomachinery Technical Conference and Exposition*, Vol. 49804, American Society of Mechanical Engineers Digital Collection, 2016, p. V05CT12A006.

[15] Oliver, T. A., Anderson, J. B., Bogard, D. G., Moser, R. D., and Laskowski, G., "Implicit LES for shaped-hole film cooling flow," *Turbo Expo: Power for Land, Sea, and Air*, Vol. 50879, American Society of Mechanical Engineers, 2017, p. V05AT12A005.

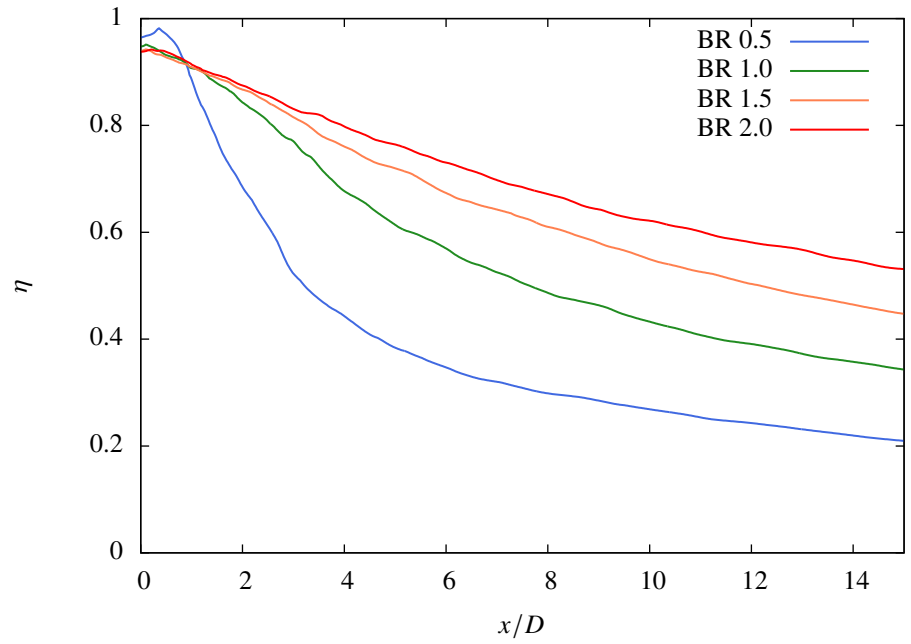

Fig. 15 Surface effectiveness η at the centerline in the flat plate region. The figure compares various blowing ratio configurations. x/D is measured from the downstream edge of the hole.

[16] Oliver, T. A., Bogard, D. G., and Moser, R. D., "Large eddy simulation of compressible, shaped-hole film cooling," *International Journal of Heat and Mass Transfer*, Vol. 140, 2019, pp. 498–517.

[17] Sudesh, A., Boehler, M., and Turner, M. G., "CFD Simulation of Flat Plate Film Cooling of Shaped Hole Using LES," *AIAA Propulsion and Energy 2019 Forum*, 2019, p. 4090.

[18] Zamiri, A., You, S. J., and Chung, J. T., "Large eddy simulation of unsteady turbulent flow structures and film-cooling effectiveness in a laidback fan-shaped hole," *Aerospace Science and Technology*, Vol. 100, 2020, p. 105793.

[19] Foster, N. W., and Lampard, D., "The flow and film cooling effectiveness following injection through a row of holes," *Gas Turbine Conference and Exhibit and Solar Energy Conference*, 1980.

[20] Ekkad, S. V., Zapata, D., and Han, J. C., "Film effectiveness over a flat surface with air and CO2 injection through compound angle holes using a transient liquid crystal image method," *Journal of Turbomachinery*, Vol. 119, No. CONF-950629-, 1997.

[21] Kohli, A., and Bogard, D. G., "Adiabatic effectiveness, thermal fields, and velocity fields for film cooling with large angle injection," *Journal of Turbomachinery*, Vol. 119, No. 2, 1997, pp. 352–358.

[22] Lu, Y., "Effect of hole configurations on film cooling from cylindrical inclined holes for the application to gas turbine blades," Ph.D. thesis, Louisiana State University and Agricultural and Mechanical College, 2007.

[23] Rozati, A., and Tafti, D. K., "Effect of coolant–mainstream blowing ratio on leading edge film cooling flow and heat transfer–LES investigation," *International Journal of Heat and Fluid Flow*, Vol. 29, No. 4, 2008, pp. 857–873.

[24] Heidmann, J. D., "A numerical study of anti-vortex film cooling designs at high blowing ratio," *Turbo Expo: Power for Land, Sea, and Air*, Vol. 43147, 2008, pp. 789–799.

[25] Cao, N., Li, X., Wu, Z., and Luo, X., "Effect of film hole geometry and blowing ratio on film cooling performance," *Applied Thermal Engineering*, Vol. 165, 2020, p. 114578.

[26] Schroeder, R. P., and Thole, K. A., "Adiabatic effectiveness measurements for a baseline shaped film cooling hole," *Turbo Expo: Power for Land, Sea, and Air*, Vol. 45721, American Society of Mechanical Engineers, 2014, p. V05BT13A036.

[27] Fischer, P., Lottes, J., Kerkemeier, S., Marin, O., Heisey, K., Obabko, A., Merzari, E., and Peet, Y., *Nek5000: User's manual*, Argonne National Laboratory, 2015.

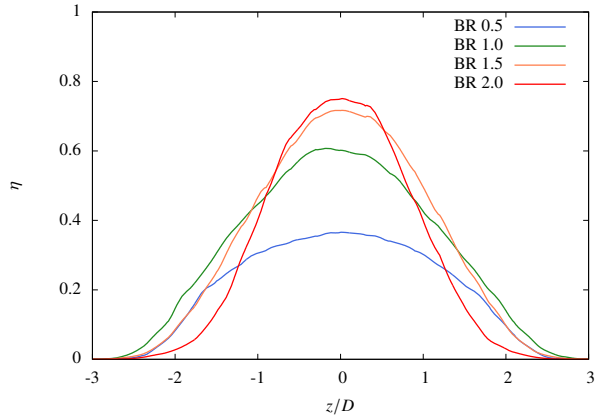

(a) $x/D = 5$

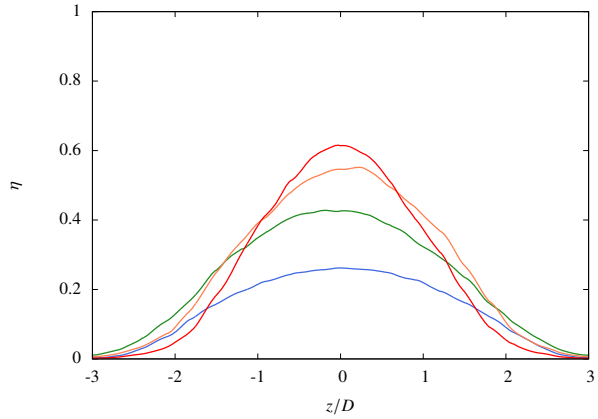

(b) $x/D = 10$

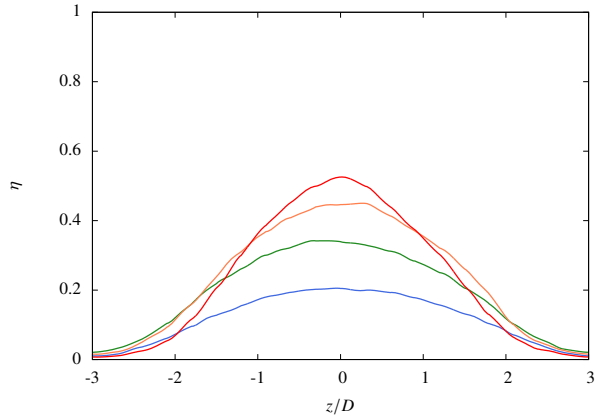

(c) $x/D = 15$

Fig. 16 Adiabatic effectiveness η over the span of the flat plate at various distances downstream of the hole. The figure compares various blowing ratio configurations. x/D is measured from the downstream edge of the hole.

(a) BR 0.5

(b) BR 1

(c) BR 1.5

Fig. 17 Normalized temperature θ in the flat plate region at $x/D = 5$ for various blowing ratios.